ARTICLES

Gas-Phase Production of Molybdenum Carbide, Nitride, and Sulfide Clusters and Nanocrystallites

James M. Lightstone,[†,‡] Heather A. Mann,[‡] Ming Wu,[†] Philip M. Johnson,[‡] and Michael G. White*[,†,‡]

Chemistry Department, Brookhaven National Laboratory, Upton, New York 11973 and Chemistry Department, SUNY Stony Brook, Stony Brook, New York 11974

Received: December 10, 2002; In Final Form: May 19, 2003

Molybdenum carbide, nitride, and sulfide clusters were created via laser ablation in the presence of dilute and neat reactive carrier gases. Distributions of the neutral products were characterized by time-of-flight mass spectrometry after photoionization with 193 nm radiation. The carbide clusters show an increase in ion intensity up to Mo_8C_{12} at which point there is a sharp drop in intensity. The latter suggests that the Mo_8C_{12} neutral or ion is particularly stable, which we attribute to a Met-Car-like structure analogous to that observed for other early transition-metal carbides. Carbide clusters containing 10−23 Mo atoms exhibit a Mo_xC_{x+3} stoichiometry, while those containing >23 Mo atoms are closer to Mo_xC_{x+2}, indicative of near cubic nanocrystallite structures. At low mass (Mo_x, $x \leq 6$), cluster ions produced in expansions of ammonia gas contained up to three nitrogen atoms; however, heavier species (Mo_x, $x \leq 40$) appear to be pure molybdenum metal clusters. The mass distributions for the sulfide clusters indicate a "magic number" structure at $Mo_6S_4^+$ which is attributed to a stable structure previously observed for the $[Cu_6S_4]^-$ anion. Also, the dependence of cluster distributions on the fluence of the ionizing laser was investigated to gain insight on the observed cluster ion distributions using a simple, qualitative kinetic model.

1. Introduction

Nanostructured compounds of molybdenum carbide, nitride, and sulfide have attracted considerable recent interest as they exhibit unique electronic and structural properties and show promise as highly active heterogeneous and photoinduced catalysts.[1−4] For example, the band gap in MoS_2 semiconductor nanoparticles varies from the visible to the near-IR over the size range of 4−10 nm making them potential catalysts for solar photoconversion reactions.[5] Under certain growth conditions, the layered nature of bulk MoS_2 also results in unusual nanostructures such as nested fullerene-like polyhedra[6] and nano/micro tubes.[7,8] In Mo_2C, recent measurements by Suslick and co-workers[3,9] have shown that high surface area aggregates of 2-nm particles catalyze gas-phase dehydrogenation reactions with an activity and selectivity comparable to that of Pt metal powder. Several synthetic approaches to nanoparticles have been used including inverse micelles,[5] laser ablation,[6] and sonochemical,[3,9,10] high-temperature,[4] and UV[11] and IR[2] induced decomposition and reaction of $Mo(CO)_6$. Generally, these approaches generate a range of particle sizes and morphologies which have been characterized by high-resolution TEM or powder X-ray diffraction.

In this work, we have investigated the formation of neutral molybdenum carbide, nitride, and sulfide clusters and nanocrystallites using a laser ablation plasma reactor. This technique has been used by many groups to explore the mass distributions, stability, and reactivity of neutral and charged clusters of a wide range of transition-metal compounds consisting of a few atoms to very large particles containing more than 100 metal atoms.[12,13] Most notable are the M_8C_{12} metal carbide clusters (Met-Cars) first discovered by Castleman and co-workers, whose preferential formation is attributed to an exceptionally stable caged structure (dodecahedron).[13−18] Larger carbide "nanocrystallites" such as $M_{14}C_{13}$ (M ≡ Ti, V, Zr) have also been observed and these are identified as fragment clusters of the bulk crystal with a 1:1 stoichiometry.[12,13] Similar stoichiometry dominates for neutral nitride clusters and nanocrystallites of Ti and Zr;[19,20] however, Nb favors formation of clusters of metal atoms to which only one nitrogen atom is attached, i.e., Nb_xN.[20] In sulfur, Dance, Willet, and co-workers observed anionic sulfide clusters containing early to late transition metals (Ni, Co, Fe, Mn, Cu, Cr, V), which are formed from laser ablation of the metal sulfide solids.[21−24] A wide range of $[M_xS_y]^-$ stoichiometries are observed, with the general trend of increasing x/y ratio with increasing number of electrons on the metal atom, for example, $x/y \approx 1$ for Mn[23] and $x/y \approx 1.6$ for Co.[24]

Despite the considerable work on metal clusters containing metals surrounding molybdenum in the Periodic Table noted above, previous laser ablation studies on molybdenum compounds are limited to the observation of cationic carbide species by Pilgrim and Duncan.[25] In that work, the $Mo_8C_{12}^+$ met-car cation is the most intense feature; however, it is less prominent than in the mass spectra of the cationic carbide clusters of first-

* Corresponding author. E-mail: mgwhite@bnl.gov.
† Brookhaven National Laboratory.
‡ SUNY Stony Brook.

10.1021/jp027674b CCC: $25.00
Published on Web 08/30/2003

row transition metals. Differences between the cation and neutral cluster distributions have been observed, most notably for neighboring Nb, for which the neutral Nb_8C_{12} cluster is comparable in intensity to surrounding clusters, whereas the $Nb_8C_{12}^+$ cation is the most prominent peak in the cation mass distribution.[26] Other gas-phase cluster studies have focused on the reactions of bare Mo_x metal clusters with various reactants which, in general, do not lead to molecularly bonded clusters.[27,28]

Here, we use laser ablation plasma reactor in conjunction with time-of-flight mass spectrometry to generate and characterize the neutral cluster distributions of molybdenum carbide, nitride, and sulfide. The cluster distributions show stoichiometries intermediate between the early and late transition metals, including the formation of "magic numbers", for example, Mo_8C_{12} and Mo_6S_4, which have previously been identified as stable cage structures.

2. Experimental Section

Neutral clusters studied in this work were produced by a Smalley-type ablation source mounted onto the front of a pulsed molecular beam valve (General Valve, Series 9). The latter delivered the reactive gases (methane, ammonia, hydrogen sulfide) required for metal compound formation within the laser-induced plasma. Both neat and dilute (5−10% in helium, 210 kPa) samples were used, with the neat expansions of methane and ammonia resulting in cluster distributions extending to higher mass. The fourth harmonic (266 nm) of a Nd:YAG, Q-switched laser (Quanta-Ray, DCR1A, 10 Hz, ∼20mJ/pulse) was used for ablation of the molybdenum rod which was continuously translated and rotated to ensure a fresh surface. The 266-nm light was focused onto the molybdenum rod with an 18-cm focal length lens. A 0.128-cm diameter stainless steel condensation channel extending approximately 4.3 cm past the focus of the ablation laser provided a confined high-pressure region for cluster formation and cooling. The molecular beam exiting the condensation tube is collimated by a 3-mm diameter skimmer and enters the ionization chamber where it interacts with 193-nm radiation from an ArF excimer laser (GAM, EX10) at the center of the extraction region of a linear (90-cm) time-of-flight mass spectrometer (TOF-MS) lying perpendicular to both the molecular and laser ionization beams. A 150-mm focal length lens was used to collimate the 193-nm light beam such that the focal point was placed before the intersection with the molecular beam. Placing the laser focus at the center of the interaction region resulted in significantly lower ion signals, which we attribute to multiple-photon fragmentation pathways caused by the increased power density (fluence). The 193-nm pulse energy was varied from 2 to 7 mJ to investigate the effects of dissociative ionization and multiphoton contributions to the observed ion distributions.

Cluster ions produced by single- or multiphoton ionization by 193-nm light were extracted by a three-element acceleration lens using Wiley−McLaren focusing conditions and detected by a dual microchannel plate (MCP) particle multiplier. Typical extraction fields were 500 V/cm with a total acceleration relative to ground potential of 2700 V. To improve the collection efficiency of heavier clusters (>1000 amu), a deflection lens element located at the entrance to the field-free region of the TOF-MS was used. The applied field opposes the transverse component of the ion's kinetic energy due to motion along the molecular beam direction and is particularly useful for accentuating the high mass region of the cluster distributions. Time-of-flight spectra were generated by recording the amplified signal from the MCP detector on a computer-controlled 20 MHz digitizer triggered by the 193-nm ionization laser pulse.

The reaction gases, methane, ammonia, and hydrogen sulfide, were obtained commercially and used without further purification.

3. General Aspects of Fluence Dependence Measurements

To facilitate the discussion of the measured fluence dependence of the cluster ion yields shown below, we present a simple kinetic model that describes the ionization and dissociation processes that are likely to contribute to the observed ion yields. Elements of this model can be found in earlier studies of multiphoton-induced ionization and dissociation of metal clusters.[29,30] Based on the expectation that all but the smallest Mo_x and Mo_xA_y (A ≡ C, N, S) clusters will have IPs less than the 6.4 eV ionization laser, the analysis is restricted to single-photon ionization but explicitly includes the possibility of photodissociation following ionization via an incoherent two-photon process. The rate expression for the yield of cluster ions with mass, m, can then be written

$$\frac{dA^+_m}{dt} = k^i_m F^i_m A_m + \sum_{n>m} k^i_n f_m(n) A_n - k^d_{m+} G^d_{m+} A^+_m + \sum_{n^+>m^+} k^d_{n+} g_{m+}(n^+) A^+_n \quad (1)$$

where A_m and A^+_m refer to the neutral and ionic cluster densities, and k^i_m and k^d_{m+} represent rate constants for one-photon ionization of the neutral cluster and one-photon, photodissociation of the cluster cation, respectively. The rate constants, k^i_m and k^d_{m+}, have the form $I_0\sigma^i_m$ and $I_0\sigma^d_{m+}$, where I_0 is the probe laser fluence and σ^i_m and σ^d_{m+} are the total neutral ionization and cation dissociation cross sections, which are assumed to be independent of fluence. Generalization to higher order processes (n) simply requires replacement of I_0 by $(I_0)^n$ and the inclusion of terms similar to those shown in eq 1 requiring all possible orders. The first and third terms of eq 1 (hereafter referred to as I and III) represent the direct ionization of the neutral cluster to form the parent ion (I) and the loss of the parent ion due to dissociation induced by subsequent photon adsorption (III). Here, the coefficient, F^i_m, represents the fraction of parent ions that remain following one-photon ionization of the neutral cluster, whereas G^d_{m+} is the total fraction of the parent ions lost to dissociation by subsequent photon adsorption. Contributions from dissociative ionization and cation photodissociation of higher mass clusters are given in the second (II) and fourth (IV) terms of eq 1, where $f_m(n)$ and $g_{m+}(n^+)$ are the dissociation fractions into specific fragments via dissociative ionization of the neutral (II) and one-photon dissociation of the cation (IV).

A more complete analysis must also include neutral fragmentation processes, which affect the densities of the neutral clusters, A_m. These processes include direct photodissociation of the neutral cluster and photodissociation and dissociative ionization of clusters of higher mass which generate a neutral fragment of mass, m. The effect of these processes are expected to be important only at very high-laser fluences where the laser-induced changes in neutral densities are comparable to the neutral cluster densities in the molecular beam (within the laser focal volume).

The time dependence of both the neutral and cation densities, coupled with the complete lack of information on cross sections and fragmentation probabilities, makes it difficult to consider limiting conditions under which the general rate expression could be integrated to obtain relative yields. Nonetheless, the

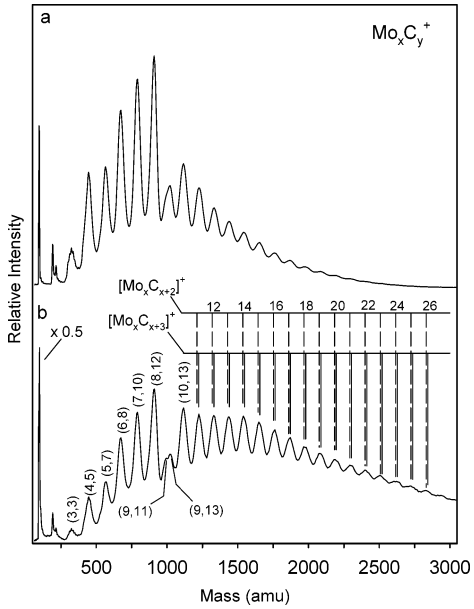

Figure 1. Time-of-flight mass spectra of $Mo_xC_y^+$ cluster ions produced by 193-nm photoionization of neutral clusters formed by 266-nm ablation of Mo metal in the presence of (a) 9% CH_4 in helium; (b) neat CH_4. All other experimental conditions the same.

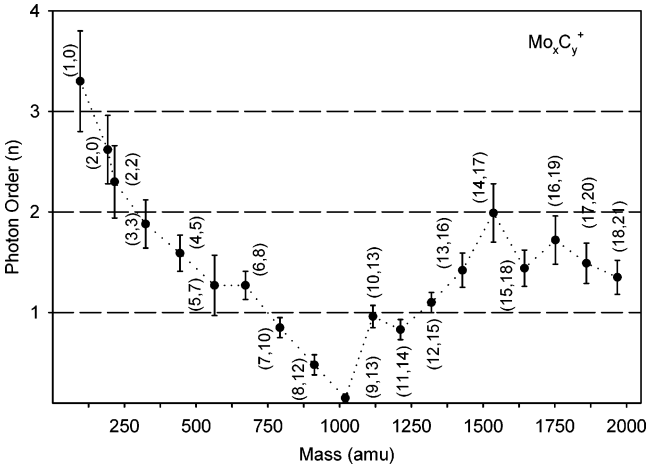

Figure 2. Fluence dependence of $Mo_xC_y^+$ cluster ion yields produced via 193-nm photoionization. The error bars reflect the quality of the least-squares fits and do not include uncertainties in the intensity measurements.

general rate expression should provide a reasonable description of the instantaneous change in cluster ion yields that can be used to make a few qualitative points concerning their expected power dependence. Specifically, terms I and II scale linearly with probe laser fluence, whereas terms III and IV, which depend on the ion densities generated by one-photon ionization, will exhibit a quadratic dependence (i.e., $\propto I^2_0$). This higher order dependence on fluence will make cation photodissociaton processes more important as the fluence is increased. Furthermore, terms I, II, and IV lead to increases in the ion yield with increasing laser fluence, whereas term III, describing photodissociation of the parent cation, results in an increasingly negative contribution. Clearly, the overall fluence dependence of any cluster ion will depend sensitively on the various contributions contained in I−IV and will not generally conform to a simple limiting case of linear or quadratic behavior. Such limiting behavior may extend over small ranges of laser fluence, for example, linear dependence at low fluences, but fractional orders are quite commonly observed in the photoionization detection of metal-containing clusters, and as shown below, sublinear behavior is also possible for specific systems.

4. Results and Discussion

4.1 Molybdenum Carbide. Mass spectra obtained by 193-nm photoionization of neutral molybdenum carbide clusters are shown in Figure 1. Both spectra were obtained under similar conditions with only the concentration of the reactant gas being varied. When dilute methane was used (Figure 1a), the largest cluster detected contained around twenty-one molybdenum atoms while the use of neat methane (Figure 1b) produced clusters containing more than twenty-six molybdenum atoms in detectable quantities. In addition, the experiments involving neat methane produce greater intensities of the higher mass clusters as well as increased yield of the molybdenum atom.

The smallest observed carbon-containing ions are Mo_2C^+ and $Mo_2C_2^+$ which appear as shoulders on the high mass side of the Mo_2^+ dimer mass peak. The next mass peak shows partially resolved structure separated by ~12 amu, which is assigned to $Mo_3C_x^+$ clusters ($x = 2-6$) with the (3,3) cluster being the most intense. Although the isotopic distribution of the Mo atoms[31] results in considerable broadening of each carbide mass peak, the substructure on the $Mo_3C_x^+$ peak suggests that the prominent mass peaks in Figure 1 correspond to a cluster with a fixed number of Mo atoms and a small range of carbon atoms. For clusters with 10 or fewer Mo atoms, the assignments in Figure 1 correspond to the peak center. As the peak widths increase for the heavier clusters, unambiguous assignments are not possible. For clusters containing 10−22 Mo atoms, the average separation of the peak midpoints is 107 ± 3 amu, which is consistent with sequential MoC addition. Starting at (10,13), this results in a cluster series with a stoichiometry of Mo_xC_{x+3} as shown by the labeling in Figure 1b. We also show the calculated mass positions for Mo_xC_{x+2} clusters, which appear to lie at the most intense part of the mass peak for very large clusters (>23 Mo atoms).

Fluence dependence measurements for the molybdenum carbide clusters are summarized in Figure 2. Here, we show the apparent photon order (n), obtained from a least-squares fit of the cluster ion peak intensity versus 193-nm fluence. Results for clusters larger than (18,21) are not shown, as the large background contribution resulted in unreliable estimates of the cluster ion peak intensities.

Theoretical estimates and direct experimental measurements indicate that the ionization potentials (IPs) of the Met-Car species for several metals (Ti, V, Zr, Nb) are less than the IP of the metal and generally lower than 6 eV.[13,32−37] Although the IP for the Mo atom (7.09 eV) is somewhat higher than these other metals, the 193-nm (6.4 eV) ionization laser used here should result in one-photon ionization of the heavier neutral species, whereas the Mo atom and dimer and the first few carbide clusters should require at least two photons for ionization. These expectations are generally consistent with the observed fluence dependence shown in Figure 2. For the Mo atom, Mo_2 dimer, and clusters up to (4,5) the derived photon orders are greater than two, indicating an IP > 6.4 eV and/or contributions from cation dissociation of larger cluster species, i.e., term IV in eq 1. Carbide cluster ions with 5, 6, 7, 10, 11, and 12 Mo atoms exhibit near linear dependence on fluence, suggesting that one-photon processes (terms I and II) dominate the formation of these cluster ions. Carbide clusters containing more than 12 Mo atoms exhibit an increase in apparent photon order, which we again ascribe to increased contributions from cation photodissociation of larger clusters (term IV).

In Figure 1a and 1b, the ion intensities for the low-mass clusters increase to the (8,12) species, beyond which there is a sharp drop in cluster signal intensity. The small mass peak following (8,12) also exhibits discernible broadening which, in the pure methane spectrum of Figure 1b, can be assigned to (9,11) and (9,13) cluster ions. These observations suggest that the (8,12) cluster is particularly stable, such that addition of another Mo atom or $MoC_{(1-2)}$ unit is unfavorable (kinetically or sterically) or unstable with respect to dissociative ionization or both. In this respect, molybdenum is similar to other early transition-metal carbides (e.g., Ti, V, Zr, Hf) which Castleman and co-workers have shown form unusually stable M_8C_{12} neutral clusters, the so-called Met-Cars, whose proposed structure is that of a hollow dodecahedron cage (T_h, T_d, or D_{2d} symmetry).[13−18] As seen in Figure 1b, the molybdenum carbide neutral mass distribution is fairly smooth over the entire range of cluster sizes, with the exception of the abrupt intensity drop for clusters containing nine molybdenum atoms. Similar behavior has been observed in the neutral mass distribution of several transition-metal carbides, particularly at low-laser fluences (Ti, V, Zr, Nb).[12,14,32] Here, the (9,11) cluster has the same number of atoms as the proposed Met-Car, suggesting the displacement of a carbon atom with a molybdenum atom. In the (9,13) species, the additional MoC unit or the C-atom could reside inside the Met-Car (endohedral) instead of lying on the surface of the cage, as previously suggested for the location of the excess carbon atom in the $[M_8C_{13}]^+$ ion observed in photodissociation experiments[38,39] and predicted by theory.[36] The intensity rise from the (9,13) to the (10,13) cluster may signal the opening of the Met-Car cage and the formation of a new structure whose stability varies only slowly with MoC_2 or MoC_3 addition, giving rise to the smooth intensity profile for heavier clusters.

The abrupt intensity variation between the (8,12) and (9,13) ions is also associated with marked, sublinear ($n < 1$) fluence dependence for these two cluster ions. As noted above, we presume that the IP of neutral Mo_8C_{12} is below the energy of the ionizing laser (6.4 eV); hence, a linear dependence on the 193-nm fluence similar to that observed for the 5, 6, 7, 10, 11, and 12 Mo atom carbide clusters might be expected. An IP greater than 6.4 eV or contributions from the fragmentation of heavier clusters would in fact yield a higher order fluence dependence ($n > 1$). According to eq 1, a sublinear fluence dependence for the (8,12) cluster could result from increased contributions from term III which represents loss of the parent ion because of photodissociation induced by the adsorption of additional photons. The latter would require that the (8,12) cation have strongly absorbing excited electronic states at 6.4 eV above the distribution of ground-state levels produced by the initial photoionization step. The existence of such levels is plausible given the high density of electronic states expected for a system containing eight molybdenum atoms. In fact, photodissociation experiments by Pilgrim and Duncan showed that the $Mo_8C_{12}^+$ cation readily adsorbs 532-nm photons to fragment by sequential MoC_2 loss.[40] Why sublinear fluence dependence is only seen for the (8,12) and (9,13) cations, however, is likely due to the unique electronic properties of the high-symmetry Met-Car structures (T_d) which we have tentatively assigned to these clusters. The fact that the derived photon order for the (9,13) ion signal is even lower than the (8,12) cation (see Figure 4) is consistent with the destabilizing effect of the additional MoC unit on the Met-Car structure which could lead to a higher probability for photoinduced fragmentation (and lower n).

Sublinear plateaus in fluence dependence measurements have also been reported by Castlemen and co-workers for the multiphoton ionization of Ti and mixed-Ti/Zr Met-Cars using low-energy photons for ionization (532 and 355 nm).[13,41,42] These observations were attributed to the competition between direct ("prompt") ionization and delayed ionization induced by internal energy conversion of "hot" molecules generated by multiphoton excitation. Delayed ionization is most likely to be significant when using low-photon energies at high fluence, which maximizes the probability for multiphoton excitation of the neutral cluster.[43] Although delayed ionization is less likely in the present work where higher energy photons (6.4 eV) and modest fluences are used, power dependence (Figure 2) alone cannot distinguish between the possible mechanisms, i.e., delayed ionization versus photodissociation of the cation (term III). In fact, attributing the observed sublinear fluence dependence to delayed ionization would only strengthen the case for the (8,12) and (9,13) clusters having unusual electronic and structural properties, for example, Met-Car-like structures.

By way of comparison, Pilgrim and Duncan previously investigated the mass distribution of the molybdenum carbide *cation* clusters generated by laser ablation.[25,44] In that work, cluster ions produced by the laser ablation source were mass analyzed using pulsed acceleration fields to provide a well-defined time zero for time-of-flight mass spectrometry. The $Mo_8C_{12}^+$ Met-Car is the dominant peak in the cation spectrum, but like the neutral data in Figure 1, the surrounding cluster peaks have substantial relative intensity. On a more detailed level, the cation and neutral mass distributions show significant differences in cluster stoichiometry and intensity distributions. Specifically, the (9,13) peak is significantly more intense in the cation spectrum, suggesting that this cluster is no less stable than the (7,9) or (11,15) species which have comparable intensity. Furthermore, the second most adundant species in the cation spectrum is the (7,9) cluster, whereas the (7,10) cluster ion is observed for photoionization of the neutrals. At higher mass, the assigned cation clusters have more carbon atoms, for example, (13,19), than the $Mo_xC_{(x+2)}$ and $Mo_xC_{(x+3)}$ species which we have proposed for the heavier clusters in the neutral photoionization mass spectrum. Such differences between the cation and neutral cluster distributions generated from laser ablation sources have been noted previously and have been attributed to differences in cluster growth mechanisms.[26,45] In the case of niobium carbide, Castleman and co-workers found that the neutral and cation distributions are completely different, with the cation distributions showing strong dependence on source conditions (e.g., hydrocarbon gas dilution).[26] For neutral molybdenum carbide clusters, large changes in the concentration of methane (see Figure 1) modify only the relative yield of the high mass clusters, but the stoichiometry of the clusters remains unchanged. Although cation distributions under other source conditions were not presented in the work of Pilgrim and Duncan,[25] the differences between the cation and neutral cluster distributions are most likely associated with ionic versus neutral growth mechanisms in the laser ablation source.

The smooth mass distribution for larger Mo_xC_y ($x > 10$) clusters with no apparent magic numbers is in contrast to that observed for the neutral carbide clusters of other early transition metals, including Zr[17,44] and Nb[26] which neighbor Mo in the periodic table. Several forms have been suggested for these higher mass species: tubes, substituted fullerenes, extended Met-Cars, and crystal fragment structures.[12,13,26,40,44] Of these, the most commonly accepted are cubic structures resembling fragments of a bulk fcc crystal lattice. These "nanocrystallites" have near 1:1 stoichiometry with sizes that range from the (14,13) cluster, which represents a [3 × 3 × 3] fcc fragment,

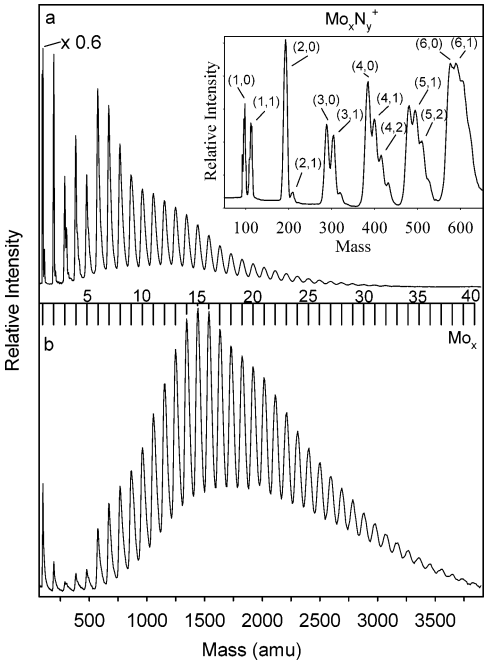

Figure 3. Time-of-flight mass spectra of $Mo_xN_y^+$ cluster ions produced by 193-nm photoionization of neutral clusters formed by 266-nm ablation of Mo metal in the presence of neat ammonia. Deflection plates on spectrometer set to (a) 270 V; (b) 320 V. Inset shows the presence of adsorbed nitrogen atoms for nitride clusters with $x < 6$.

to the largest observed [7 × 6 × 6] cubic fragment associated with the $Ti_{126}N_{126}$ cluster.[19] As noted earlier, the heavier mass peaks for molybdenum carbide likely contain contributions from both $[MoC_{x+2}]^+$ and $[Mo_xC_{x+3}]^+$ ions, neither of which exhibit the exact 1:1 stoichiometry expected for fcc nanocrystallites. In the case of Ti, Pilgrim and Duncan assigned the near 1:1 carbide cation clusters, (17,19), (23,25), and (31,33), to cubic structures as the only reasonable alternative.[40,44] The latter have the same $M_xC_{(x+2)}$ stoichiometry proposed for the higher clusters of molybdenum (Figure 1b) and it is reasonable to assign these to nanocrystallites. Unlike the bulk carbides of Ti, V, Cr, Hf, Zr, and Nb which have fcc crystal structures,[46] however, molybdenum carbide has a complex phase diagram which includes several stable and metastable equilibrium phases.[47] At room temperature, there are two types of Mo_2C (α orthorhombic, β hexagonal) and the hexagonal γ-MoC structures, while the cubic δ-MoC (NaCl-type) and hexagonal η-MoC phases exist only at high temperatures and are nonstoichiometric, i.e., $MoC_{1-x.}$ In large part, different phases of the same stoichiometry represent various levels of disorder of the interstitial carbon atoms. It is possible that the larger Mo_xC_y ($y = x + 2,3$) clusters have simple cubic (δ-MoC) or hexagonal (γ-MoC) structures; however, the ability of molybdenum metal to accommodate carbon over a wide range of order and stoichiometry may preclude the formation of such simple structures given the extreme conditions of the ablation source.

4.2 Molybdenum Nitride. Mass spectra of molybdenum nitride clusters are shown in Figure 3. The use of neat ammonia helped promote the growth of larger clusters (up to 40 Mo atoms) as well as provided greater cluster intensities as compared to dilute ammonia, as seen in the carbide clusters. By adjusting the voltage on the deflection plates, specific mass ranges of the cluster ions could be enhanced by steering them through the TOF-MS. The deflection voltage compensates for the beam velocity of the clusters perpendicular to the TOF-MS detection axis. The spectra in Figure 3 were obtained using the same ablation and ionization laser powers and varying the deflection

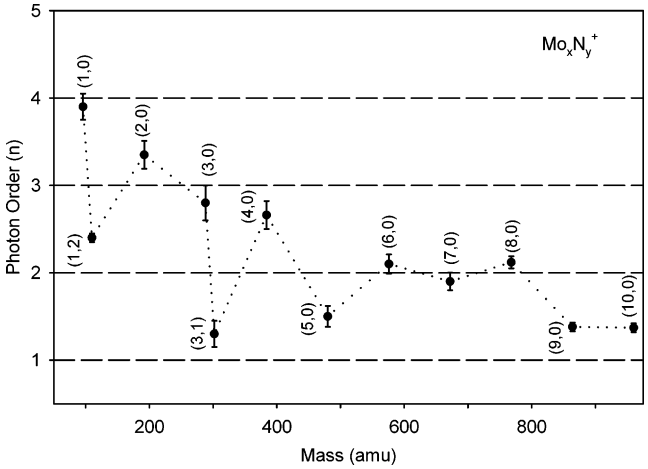

Figure 4. Time-of-flight mass spectra of Mo_xS_y cluster ions produced by 193-nm photoionization of neutral clusters formed by 266-nm ablation of Mo metal in the presence of 9% hydrogen sulfide in helium.

plate voltage from 260 V (top panel) to 320 V (lower panel). Tuning the deflection plate voltages skews the overall intensity distribution of the mass spectrum, while preserving the ratios of neighboring peaks. Similar behavior was also observed for the carbide species.

Cluster ions formed from molybdenum and ammonia have stoichiometries very similar to that observed by Kooi and Castleman for neutral niobium nitride clusters using a laser ablation plasma reactor.[20] In that work, only bare Nb_x and Nb_xN clusters are found which they attribute to the complete dehydrogenation of ammonia in the laser plasma leaving free nitrogen atoms available for cluster formation. In contrast, the nitride clusters of Ti and Zr form a wider range of stoichiometries with the most probable being the 1:1 cluster, i.e., M_xN_x.[20] In the present experiment, molybdenum clusters of lower mass follow a similar trend as Nb; however, because of the larger isotopic distribution of the molybdenum atom it is difficult to resolve nitride species above the $Mo_6N_x^+$ clusters. The presence of nitride clusters is seen more clearly in the inset of Figure 3, where individual nitrogen additions are partially resolved. For these small cluster ions, the intensity drops rapidly with sequential addition of N-atoms. The latter may reflect the relative stability of the $Mo_xN_{(1-3)}$ neutral clusters, as well as the influence of dissociative processes leading to loss of the parent cation induced by the 193-nm ionization laser.

As the number of molybdenum atoms increase, the ability to resolve the nitrogen adatoms is lost and the peak centers correspond to bare molybdenum clusters. Slight asymmetries in the high mass peak shapes and the presence of nitride clusters at lower mass makes the presence of high-mass Mo_xN_y ($x > 10$, $y = 1-3$) species plausible. Large Mo_x clusters with one or two nitrogen adatoms approaches the limit of bulk Mo metal with chemisorbed N-atoms at low coverage. Such clusters are similar to that formed by thermal reaction of neutral Mo_x clusters with N_2 as studied by Mitchell et al. using a fast-flow reactor and photoionization mass spectrometry (193 nm) for product detection.[27] Typical products were $Mo_x(N_2)_{1,2}$ clusters which may include both chemisorbed N-atoms and intact N_2 molecules.

The fluence dependence of the smaller Mo_x^+ and $Mo_xN_y^+$ cluster ion peak intensities are shown in Figure 4. As noted earlier, mass peaks with $x > 3$ are assigned to the bare metal clusters, Mo_x^+; however, the resolution is insufficient to exclude the possibility of closely lying Mo_xN^+ clusters. Similar to the carbide, the smallest Mo atom clusters show photon orders greater than two, which we attribute to IPs exceeding the 6.4

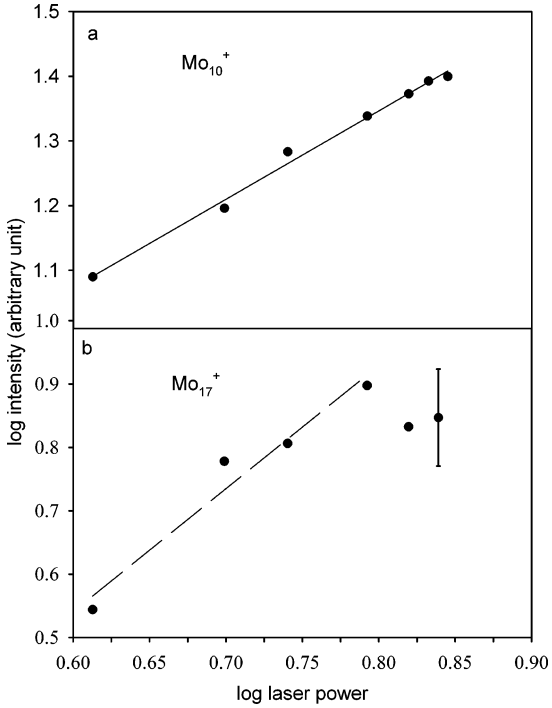

Figure 5. Fluence dependence of $Mo_xN_y^+$ cluster ion yields produced via 193-nm photoionization. The error bars reflect the quality of the least-squares fits and do not include uncertainties in the intensity measurements.

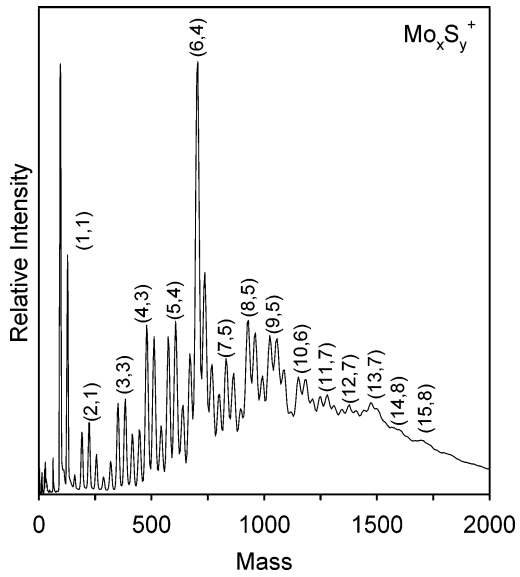

Figure 6. Example least-squares fits of cluster ion intensity versus 193-nm fluence for (a) Mo_{10}^+ and (b) Mo_{17}^+ where a plateau effect is observed for higher laser fluences. The dashed line is a fit to the first four points and resulting in a photon order of 1.81 ± 0.26, which is similar to that obtained for smaller clusters. The error bar on the last point indicates the estimated uncertainty in the intensity measurements.

eV photon energy, and contributions from cation photodissociation of larger clusters (term IV) which can generate ionic fragments of the same mass. Compared to the bare metal clusters, the MoN_2^+ and Mo_3N^+ clusters exhibit significantly lower order photon orders which could indicate lower IPs but more likely is due to smaller contributions from dissociative processes that lead to these specific nitride fragments. As the number of Mo atoms increases, the fluence dependence becomes approximately quadratic and decreases again for Mo_9^+ and Mo_{10}^+. At even higher mass, the fluence versus intensity curves exhibit plateaus at the highest fluences, such that a simple straight line fit is not possible. This is illustrated in Figure 5, where we show the fluence versus intensity fits for Mo_{10}^+ and Mo_{17}^+. The linear fit for the Mo_{10}^+ data is typical of the lower mass cluster ions, whereas the intensity of the Mo_{17}^+ mass peak reaches a maximum at higher fluence. Using only the first four points (dashed line in Figure 5), a linear fit leads to a photon order of $n = 1.81 \pm 0.26$ which is similar to that observed for the lower mass clusters. This behavior is observed to various degrees for all clusters larger than Mo_{10}^+ and is indicative of cluster ion depletion resulting from photodissociation of the cation (term III) at higher 193-nm laser fluences.

The inability to generate molybdenum nitride clusters with more than just a few nitrogen atoms is surprising given the carbide results presented above and the fact that molybdenum nitride is a well-known bulk alloy, the most stable phase being cubic (fcc) γ-Mo_2N.[46] Other bulk phases (hcp, α-MoN) and thin films (δ-MoN) have also been observed using a variety of chemical preparation methods.[49] The gas-phase results of this work and that of Mitchell et al.[27] suggest that the molybdenum clusters have a different affinity for nitrogen incorporation than the bulk metal. Alternatively, the growth mechanism and kinetics in the gas phase may limit the Mo−N interaction. For example, differences between ammonia and methane reactivity toward alloy cluster formation may reflect the stability of the carbon or nitrogen precursors in the plasma. Specifically, carbon-containing plasmas are known to contain stable C_2 species which are available for reaction. In the ammonia plasma, N-atoms or (NH_x species) are the reactive species and their lifetimes may be short because of wall collisions or N+N recombination, which could limit their interaction time with nucleating metal atoms. Experiments involving laser ablation of the bulk molybdenum nitride with and without additional nitrogen feed molecules could provide insight into the gas-phase growth mechanism and will be pursued in future work.

4.3 Molybdenum Sulfide. Despite the wealth of data on the neutral and cation carbide and nitride clusters, almost no such information exists for the sulfide clusters of the early transition metals even though most form stable bulk sulfides, generally of the form MS_2. A wide range of metal sulfide clusters have been observed as anions, however, by Dance and co-workers using laser ablation of the bulk sulfide and ion cyclotron resonance mass spectrometry.[21−24,49−52] Of particular interest is the observation of abundant anion clusters of specific stoichiometry, for example, $[Co_xS_x]^-$ and $[Cu_xS_{(x-2)/2}]^-$, some which are attributed to particularly stable caged cluster geometries, similar in many respects to that found for the neutral and cation Met-Car species.[24,50−52]

The photoionization mass spectrum of the Mo_xS_y clusters formed using a 9% mixture of H_2S in He as the reactant gas is shown in Figure 6. Because of the larger atomic weight of sulfur, individual cluster species are more readily resolved; however, specific assignments are complicated by the coincidental mass equivalence of three sulfur atoms and one molybdenum atom (average atomic weight of 96 amu). The assignments given in Figure 6 are based on the trend of consecutive single molybdenum atom addition observed for the nitride and carbide clusters and the comparison with the work by Dance et. al. on $[Cu_xS_y]^-$ cluster anions.[49,52] The latter provided a means to make reasonable mass assignments for a few of the most prominent Mo_xS_y mass peaks, which in turn fixes the stoichiometry of other nearby mass peaks. Specifically, the stoichiometry of species that differ by one sulfur atom from the labeled clusters are uniquely determined; however, because of the 3:1 mass coincidence, species differing by more than one sulfur atom

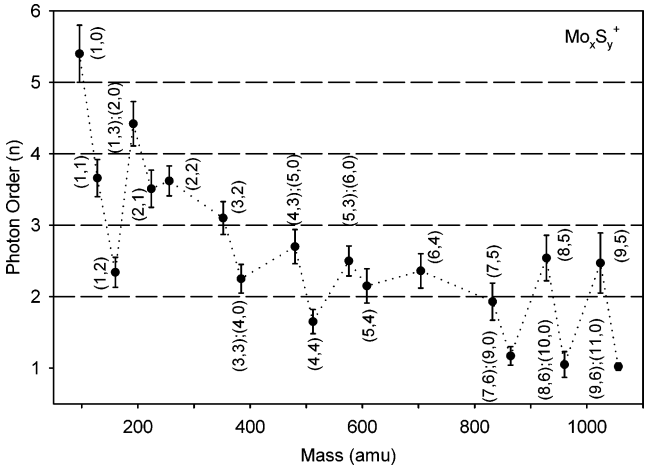

Figure 7. Fluence dependence of $Mo_xS_y^+$ cluster ion yields produced via 193-nm photoionization.

may have contributions from other sulfide clusters with different numbers of Mo atoms.

The most abundant cluster ion is $Mo_6S_4^+$ and the largest resolvable cluster is $Mo_{15}S_8^+$. Ion intensity extends to even higher mass, but features beyond the (15,8) cluster are evidently very broad. As noted above, assignment of the largest ion peak to the (6,4) cluster is based on similarities with the copper sulfide anion mass distributions obtained by Dance and co-workers using laser ablation of the bulk sulfide.[49,52] The stability of the $Cu_6S_4^-$ anion was attributed to a stable cage structure involving an octahedral arrangement of the Cu atoms onto which the S-atoms are attached on four sides. The stability of the $[Cu_3S_3]^-$, $[Cu_6S_4]^-$, and $[Cu_{10}S_6]^-$ cluster anions was argued to arise from local S−Cu−S linear (or near-linear) coordination.[52] The abundance of the $Mo_6S_4^+$ cation (Figure 6) relative to those clusters with (±1 S)-atom is quite striking and very different than all other cluster ions with different numbers of Mo atoms. These observations coupled with similar findings for the copper anion clusters suggest that the Mo_6S_4 species is a "magic number" cluster (cation and neutral) with a particularly stable geometry. The fact that the $Mo_3S_3^+$ and $Mo_{10}S_6^+$ cluster ions do not also appear with enhanced yields is most likely a reflection of the different metal sulfide stabilities, i.e., Mo versus Cu, which is analogous to the differences observed in the mass distributions for different early transition-metal carbides and nitrides.

Beyond the (6,4) cluster ion there appears to be a trend toward an increased molybdenum-to-sulfur ratio with increasing cluster size. This observation could be attributed to a wider range of stable sulfide species for a specific number of molybdenum atoms, the loss of sulfur atom during ionization, or contributions from the fragmentation of higher molecular weight clusters via dissociative ionization. In this regard, it is also interesting to contrast loss of mass resolution observed for the sulfide clusters near 1500 amu (Figure 7) versus 2500 amu in the carbide spectrum (Figure 1) even though the separation between sequential cluster masses is smaller (12 vs 32 amu). The latter suggests a much larger contribution from dissociative processes in the sulfide mass spectrum, which could contribute to the nearly continuous background distribution of cluster ions.

The dependence of the $Mo_xS_y^+$ peak intensities on the 193-nm laser fluence is summarized in Figure 7. The overall behavior is very similar to that observed for the Mo_x^+ and $Mo_xN_y^+$ clusters (Figure 4) with the smallest ion species exhibiting high-order fluence dependence that decreases to approximately quadratic behavior for clusters up to 10 Mo atoms. Again, the observation of $n > 2$ for the Mo-atom, dimer, and smaller sulfides species is indicative of IPs greater than 6.4 eV as well as a signature of contributions from cation photodissociation of heavier clusters (term IV). The latter would also explain the quadratic dependence observed for cluster ions larger than (3,3). The rapid variation of the photon orders between the peaks assigned to (7,6) and (9,6), is in large part a result of saturation in the peak intensities at higher fluences similar to the Mo_x^+ data shown in Figure 5. This behavior is more prominent for heavier clusters where simple straight-line fits did not provide a meaningful photon order and these data are not included in Figure 7. The fact that the three ion peaks labeled (7,6), (8,6), and (9,6) exhibit lower photon orders than their neighboring peaks can be rationalized by assigning these ions to bare Mo_x^+ clusters with $x = 9$, 10, and 11 (as a result of the 3:1 mass equivalency of Mo to S atoms). This alternative assignment is supported by similarities of the observed fluence dependence for the mass peaks corresponding to Mo_9^+ and Mo_{10}^+ in both the sulfide and nitride data.

5. Summary

Neutral cluster distributions of molybdenum carbide, nitride, and sulfide were produced by a laser plasma ablation source and probed by photoionization mass spectrometry using UV radiation at 193 nm and time-of-flight mass spectrometry. Using methane as the carbon source, carbide clusters ions containing up to 26 Mo atoms were observed, with an intensity break at the (8,12) ion. We interpret the latter as indicative of the stability of the (8,12) neutral cluster, analogous to the stable M_8C_{12} neutral and cation Met-Car species observed for many of the other early transition metals. Carbide clusters of higher mass appear with a stoichiometry of (x, $y = x + 2$) or (x, $y = x + 3$), which we tentatively assign to near cubic nanocrystallites, are also similar to that observed for other transition-metal carbides. The nitrides behave very differently, with the bare Mo_x^+ clusters being most abundant ($x \leq 40$), with evidence at low mass for nitride cluster ions with only 1−3 nitrogen atoms attached. The sulfide photoionization mass spectrum exhibits a very prominent peak, which we assign to the $Mo_6S_4^+$ cluster ion on the basis of similarities with copper sulfide anion mass distributions. The enhanced stability of the (6,4) sulfide cluster is attributed to caged structure analogous to the Met-Cars and suggests that other neutral metal sulfide clusters may exhibit structurally based "magic numbers". Fluence dependence measurements are interpreted on the basis of a simple kinetic model, which provides a rationale for the observed complex behavior of the cluster intensities versus fluence and size. Generally, cation fragmentation induced by the adsorption of additional photons appears to be the most important process in determining the overall fluence dependence of the cluster ion intensities. For small clusters ($x \leq 5$), this leads to increases in the apparent photon order ($n \geq 2$), whereas for the large clusters of the nitride and sulfide ($x > 10$), fragmentation of the parent cations results in saturation of the ion signals at high fluences. The sublinear fluence dependence of the (8,12) and (9,13) Met-Car ion intensities over the entire fluence range studied can also be attributed to photoinduced fragmentation and is at least partly responsible for the modest abundance of the (8,12) cation observed in the mass spectrum. Although higher energy photons (6.4 eV, 193 nm) are used here to reduce the probabilities of dissociative and delayed ionization processes, the fluence dependent measurements indicate that the observed cluster ion distributions are only a qualitative measure of the neutral mass distribution produced by the laser ablation source. Nonetheless,

the redisitribution of cluster ion intensities resulting from cation fragmentation is not sufficient to alter the conclusions concerning the stability of specific cluster species, such as the Mo_8C_{12} Met-Car and Mo_6S_4.

Acknowledgment. The authors would like to thank Prof. Arthur Suits for the use of his excimer laser which provided the 193-nm radiation for photoionization of the neutral clusters. This work was supported by the U.S. Department of Energy, Office of Basic Energy Sciences, Division of Chemical Sciences under contracts No. DE-AC02--98CH10886 (J.M.L., M.W., M.G.W.) and FG02-86ER13590 (H.M., P.M.J.).

References and Notes

(1) Klabunde, K. J.; Mulukutla, R. S. Chemical and Catalytic Properties of Nanocrystals. In *Nanoscale Materials in Chemistry*; Klabunde, K. J., Ed.; John Wiley and Sons: New York, 2001; p 223.

(2) Ochoa, R.; Bi, X. X.; Rao, A. M.; Eklund, P. C. Transition metal Nitride and Carbide Nanoparticles. In *The Chemistry of Transition Metal Carbides and Nitrides*; Oyama, S. T., Ed.; Blackie Academic: Glasgow, U.K., 1996; p 489 and references therein.

(3) Suslick, K. S.; fang, M. M.; Hyeon, T.; Mdleleni, M. M. *Applications of Sonochemistry to Materials Synthesis*; Luwer: Dordrecht, Netherlands, 1999.

(4) Close, M. R.; Petersen, J. L.; Kugler, E. L. *Inorg. Chem.* **1999**, *38*, 1535.

(5) Thurston, T. R.; Wilcoxon, J. P. *J. Phys. Chem.* **1999**, *103*, 11.

(6) Parillo, P. A.; Dillion, A. C.; Jones, K. M.; Riker, G.; Schulz, D. L.; Ginley, D. S.; Heben, M. J. *Nature* **1999**, *397*, 114.

(7) Remskar, M.; Skraba, Z.; Cleton, F.; Sanjines, R.; Levy, F. *Appl. Phys. Lett.* **1996**, *69*, 351.

(8) Remskar, M.; Skraba, Z.; Regula, M.; Ballif, C.; Sanjines, R.; Levy, F. *Adv. Mater.* **1998**, *10*, 246.

(9) Hyeon, T.; Fang, M.; Suslick, K. S. *J. Am. Chem. Soc.* **1996**, *118*, 5492.

(10) Mdleleni, M. M.; Hyeon, T.; Suslick, K. S. *J. Am. Chem. Soc.* **1998**, *120*, 6189.

(11) Jin, C.; Haufler, R. E.; Hettich, R. L.; Barshick, C. M.; Compton, R. N.; Puretzky, A. A.; Dem'yanenko, A. V.; Tuinman, A. A. *Science* **1994**, *263*, 68.

(12) Duncan, M. A. *J. Cluster Sci.* **1997**, *8*, 239.

(13) Leswik, B. D.; Castleman, A. W., Jr. *J. Physique* **2002**, *3*, 251 and references therein.

(14) Guo, B. C.; Wei, S.; Purnell, J.; Buzza, S.; Castleman, A. W., Jr. *Science* **1992**, *256*, 515.

(15) Guo, B. C.; Kerns, K. P.; Castleman, A. W., Jr. *Science* **1992**, *255*, 1411.

(16) Guo, B. C.; Wei, S.; Chen, Z.; Kerns, K. P.; Purnell, J.; Buzza, S.; Castleman, A. W., Jr. *J. Chem. Phys.* **1992**, *97*, 5243.

(17) Wei, S.; Guo, B. C.; Purnell, J.; Buzza, S.; Castleman, A. W., Jr. *Science* **1992**, *256*, 818.

(18) Wei, S.; Guo, B. C.; Purnell, J.; Buzza, S.; Castleman, A. W., Jr. *J. Phys. Chem.* **1992**, *96*, 4166.

(19) Chen, Z. Y.; Castleman, A. W., Jr. *J. Chem. Phys.* **1993**, *98*, 231.

(20) Koo, S. E.; Castleman, A. W., Jr. *Chem. Phys. Lett.* **1999**, *315*, 49.

(21) Nakat, J. H. E.; Dance, I. G.; Fischer, K. J.; Rice, D.; Willett, G. D. *J. Am. Chem. Soc.* **1991**, *113*, 5141.

(22) Nakat, J. H. E.; Dance, I. G.; Fischer, K. J.; Willett, G. D. *Inorg. Chem.* **1991**, *30*, 2957.

(23) Dance, I. G.; Fischer, K. J.; Willett, G. D. *J. Chem. Soc., Dalton Trans.* **1997**, 2557.

(24) Nakat, J. H. E.; Dance, I. G.; Fischer, K. J.; Rice, D.; Willett, G. D. *Inorg. Chem.* **1993**, *32*, 1931.

(25) Pilgrim, J. S.; Duncan, M. A. *J. Am. Chem. Soc.* **1993**, *115*, 6958.

(26) Wei, S.; Guo, B. C.; Deng, H. T.; Kerns, K.; Purnell, J.; Buzza, S. A.; Castleman, A. W., Jr. *J. Am. Chem. Soc.* **1994**, *116*, 4475.

(27) Mitchell, S. A.; Lian, L.; Rayner, D. M.; Hackett, P. A. *J. Chem. Phys.* **1995**, *103*, 5539.

(28) Berces, A.; Mitchell, S. A.; Zgierski, M. Z. *J. Phys. Chem. A* **1998**, *102*, 6340.

(29) Amrein, A.; Simpson, R.; Hackett, P. *J. Chem. Phys.* **1991**, *95*, 1781.

(30) Brucat, P. J.; Zheng, L.-S.; Pettiette, C. L.; Yang, S.; Smalley, R. E. *J. Chem. Phys.* **1986**, *84*, 3078.

(31) Molybdenum naturally occurring isotopic distribution: 92Mo (14.84%); 94Mo (9.25%); 95Mo (15.92%); 96Mo (16.68%); 97Mo (9.55%); 98Mo (24.13%); 100Mo (9.63%).

(32) Brock, L. R.; Duncan, M. A. *J. Phys. Chem.* **1996**, *100*, 5654.

(33) Reddy, B. V.; Khanna, S. N.; Jena, P. *Science* **1992**, *258*, 1640.

(34) Grimes, R. W.; Gale, J. D. *J. Phys. Chem.* **1993**, *97*, 4616.

(35) Dance, I. *J. Am. Chem. Soc.* **1996**, *118*, 2699.

(36) Reddy, B. V.; Khanna, S. N. *Chem. Phys. Lett.* **1993**, *209*, 104.

(37) Sakuri, H.; Castleman, A. W. *J. Phys. Chem. A* **1998**, *102*, 10486.

(38) Wei, S.; Guo, B. C.; Purnell, J.; Buzza, S. A.; Castleman, A. W., Jr. *J. Phys. Chem.* **1993**, *97*, 9559.

(39) Purnell, J.; Wei, S.; Castleman, A. W., Jr. *Chem. Phys. Lett.* **1994**, *229*, 105.

(40) Pilgrim, J. S.; Duncan, M. A. *J. Am. Chem. Soc.* **1993**, *115*, 9724.

(41) Kooi, S. E.; Castleman, A. W., Jr. *J. Chem. Phys.* **1998**, *108*, 8864.

(42) Cartier, S. F.; May, B. D.; Castleman, A. W., Jr. *J. Chem. Phys.* **1996**, *104*, 3423.

(43) Knickelbein, M. B. *Philos. Mag. B* **1999**, *79*, 1379 and references therein.

(44) Pilgrim, J. S.; Duncan, M. A. *Int. J.Mass Spectrometry. Ion Processes* **1994**, *138*, 283.

(45) Sakuri, H.; Castleman, A. W. *J. Phys. Chem. A* **1997**, *101*, 7695.

(46) Oyama, S. T. Introduction to the Chemistry of Transition Metal Carbides and Nitrides. In *The Chemistry of Transition Metal Carbides and Nitrides*; Oyama, S. T., Ed.; Blackie Academic and Professional: Glasgow, U.K., 1996; p 1 and references therein.

(47) Hugosson, H. W.; Eriksson, O.; Nordstrom, L.; Jansson, U.; Fast, L.; Delin, A.; Wills, J. M.; Johansson, B. *J. Appl. Phys.* **1999**, *86*, 3758 and references therein.

(48) Marchand, R.; Gouin, X.; Tessier, F.; Laurent, Y. New Route to Mo Nitrides and Oxynitrides: Preparation and Characterization of new Phases. In *The Chemistry of Transition Metal Carbides and Nitrides*; Oyama, S. T., Ed.; Blackie Academic and Professional: Glasgow, U.K., 1996; p 252 and references therein.

(49) Nakat, J. H. E.; Dance, I. G.; Fisher, K. J.; Willett, G. D. *Inorg. Chem.* **1991**, *30*, 2957.

(50) Dance, I. G.; Fisher, K. J. *J. Chem. Soc., Dalton Trans.* **1997**, 2563.

(51) Dance, I. G. *Chem. Commun.* **1998**, 523.

(52) Fisher, K. J.; Dance, I. G.; Willett, G. D.; Yi, M. *J. Chem. Soc., Dalton Trans.* **1996**, 709.